Human Metal ESD: Design of a Full-Wave Model and an Improved Compact Generator

Guang-Xiao Luo, *Member, IEEE*, Bao-Cheng Huang, Ke Huang, *Member, IEEE*, Rui Mi, *Member, IEEE*, and David Pommerenke, *Fellow, IEEE*

***Abstract*—A full-size, full-wave human body model has been designed. Compared with a real human-metal electrostatic discharge (ESD), similar fields and currents are obtained from the numerical model. A resistive surface sheet is used in microwave studio to control the currents on the air-filled body. Its performance is verified by comparing it to the currents and fields from the real human ESD. A subcircuit models the time-dependent resistance of the spark using the well-known Rompe–Weizel spark resistance model. Real human metal ESD does not reveal the double hump shape as shown in the IEC standard. To create a generator that reproduces the real human metal ESD current waveform, a compact ESD generator was designed, which is based on matching the impedance of real human metal mode ESD with the impedance of the compact ESD generator. Furthermore, a circuit-based simulator is presented. It is based on a PCB implementation of the equivalent circuit of the human metal ESD.**

***Index Terms*—Air discharge, compact generator, electrostatic discharge (ESD), full-wave model, human body, resistive surface.**

I. Introduction

MANY experimental setups have been published [1], [2], [3] for investigating the electrostatic discharge (ESD) characteristics of the human body, using circuit models and full wave models. The discharge current waveform observed when discharging a human who holds a small metal piece in his or her hand (human metal model: HMM) shows obvious differences when compared with the waveform that is used in the IEC standard generator [4]. If discharges involve a human volunteer, he or she will feel pain for voltages larger an about 5 kV. A full-sized dummy can reproduce the currents and transient fields of the human metal ESD. We recently published our findings on a full-size dummy [5], [6]. It uses a mannequin covered with conductive cloth to match the discharge current of humans holding a piece of metal. Compared with the real human ESD, similar characteristics are obtained for the discharge current and the transient fields. The emphasis of our previous paper was on discharges from a hand held metal piece which we refer to as HMM [5]. This work has been extended to also cover the discharge characteristics from the different body-worn ESD scenarios [6]. For the test scenarios in which a DUT was worn on the wrist, the elbow and the waist, the dummy designs were verified by comparing the impedance and discharge current to those of volunteer.

Numerical 3D models can form an efficient tool to predict the discharge currents and radiated fields of ESD. Most previously published work on full wave modeling of ESD treats commercial ESD generators [7], [8], [9], [10], [11]. To match air discharge, the effect of the spark needs to be included in the simulation model [12], [13]. When analyzing published models, we see four stages of the development:

- *Models without the spark resistance:* A step function was used instead of the time-dependent spark resistance to represent the internal relay of the ESD generator [7], [8], [9]. The time-dependent spark resistance was not included, but the spark effect was indirectly taken into account by setting different rise times of the step function. The geometry of the 3D models reflect commercial ESD generator with varying degree of simplification. Verification was based on comparing simulated currents and fields [7]. Additionally, the effect of different loads was considered in [8] and [9].
- *Models which include the spark resistance but need a circuit simulator, which is external to the full wave simulation. Thus, a two- or three-step process is needed:* The next publications began to include the spark resistance in a SPICE-like tool. S-parameter results are obtained using numerical full-wave simulation. These are imported into a SPICE-like tool. This yields the discharge current including the effect of the spark length [10]. Most authors use the spark resistance model from Rompe and Weizel [14]. To obtain the fields, the current needs to be reimported into the full wave solver [15] as excitation.
- *Models with field-circuit cosimulation:* In further developments, transient cosimulation was performed. Here, the full wave simulator and the spice circuit of the spark resistance model exchange information in each time step [11]. CST microwave studio (MWS) offers this option. The advantage is obtaining fields and currents in a one-step process. This is at the expense of not being able to reuse simulations that

Manuscript received 5 November 2022; revised 21 February 2023; accepted 8 March 2023. Date of publication 4 April 2023; date of current version 13 June 2023. *(Corresponding author: David Pommerenke.)*

Guang-Xiao Luo and Bao-Cheng Huang are with the Hebei Key Laboratory of Power Internet of Things Technology, North China Electric Power University, Baoding 071000, China (e-mail: guangxiao.luo@ncepu.edu.cn; 1171583177@qq.com).

Ke Huang is with the Tongji University, Shanghai 201804, China (e-mail: hk1328170662@sina.com).

Rui Mi is with the Graz University of Technology, 8010 Graz, Austria (e-mail: rui.mi@tugraz.at).

David Pommerenke is with the Graz University of Technology, 8010 Graz, Austria, and also with the Silicon Austria Laboratory GEMC lab, 8010 Graz, Austria (e-mail: david.pommerenke@ieee.org).

Color versions of one or more figures in this article are available at https://doi.org/10.1109/TEMC.2023.3257240.

Digital Object Identifier 10.1109/TEMC.2023.3257240

resulted in S-parameter blocks. The meshing efficiency of the finite integration technique and transmission line matrix is compared for a simple structure including a metal round rod [16]. Using the magnetically mixed Newmark-Leapfrog finite-difference time-domain method, the arc was included for a numerical model [17], [18].

- *Full-size full-wave human body models:* An ESD generator always forms a simplification of the actual human metal ESD. Using a full-sized full-wave model, actual ESD situations can be reproduced in simulation. A 3D full-wave human body model was described in [19] and [20]. By considering the dissipation characteristics of biological tissue, this model can be used to analyze the in-situ transient fields and currents [19]. A different approach was selected in [20], the human body was modeled as a homogeneous dielectric having a frequency-dependent complex permittivity. The effect of discharge position and posture of the human body was investigated by using the EMCoS software [20] which uses an MoM solver.

Further improvements for the full-size full-wave human body model can be achieved by

1) Inclusion of the time-dependent spark resistance to obtain the discharge current and transient fields in [19] and [20].
2) The frequency-dependent material characteristics of the body had been approximated in [19] and [20], however, the achieved match to measured reference data was only moderate.

In addition to the numerical solution path, the type of ESD event that is analyzed must also be considered. This can extend from human-skin ESD, to human-metal ESD and to discharges from body worn equipment. The discharge current waveforms of IEC standard generators are different from those of actual human metal ESD, the second hump is hardly ever seen in actual ESD. For ESD of body worn equipment it has been shown that the peak discharge current is larger than the 3.75 A/kV, the standardized peak current value of contact mode ESD [1], [21]. To recreate human metal ESD more realistic and to test body worn equipment sufficiently, new ESD generator designs are helpful [22].

Based on our previous research [5], [6], a 3D full-wave model is presented in this article. Innovations of the proposed full-wave model lie in the combination of known methods for the simulation and optimization of the ESD dummy. The features of the proposed modeling and simulation methods are as follows.

1) A modeling method is presented to simulate the impedance characteristics of real human body. To describe the real fabric cloth used in the artificial dummy design [5], [6], the ohmic sheet surface resistance is used to simplify the modeling process of the material characteristics in CST MWS. Different constant resistance values are set for the different parts of human body model. They approximate the impedance characteristics that are measured for a real human body. The effect of different human parts on the whole human body impedance is evaluated.
2) The air discharge currents and transient fields of a real human body at different voltage levels can be simultaneously predicted by using the proposed full-size full-wave dummy model. The time-dependence resistance model of spark is still represented as a subcircuit and combined with the ESD dummy model. The Rompe–Weizel spark subcircuit [23] is directly embedded into the CST MWS by a nonlinear lumped component in the transient simulation. Thus, the discharge currents, electric fields, and magnetic fields can be simultaneously obtained without involving a separated circuit simulator.

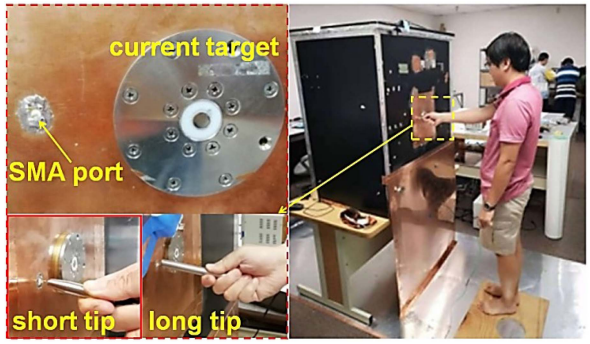

Fig. 1. Setup for air discharge testing. For impedance measurements, an VNA is used, and the current target is substituted by an SMA probe.

Furthermore, a compact electromagnetic full-wave model and a PCB-based simulator are designed. A mercury switch is used to trigger the discharge event for the circuit-based simulator. Compared with the traditional generators referencing to IEC standard [10], their impedance characteristics are more consistent with those of the real human body. The PCB-based simulator and the full-wave model of a compact ESD generator achieve similar discharge currents as the 3D full-size numerical model.

II. Full-Wave Numerical Model Design

This section describes the human body full-wave full-size numerical model and its design approach which is based on achieving similar impedances and consequent similar discharge current waveforms and transient electromagnetic fields. At first, the impedance of HMM is measured and an equivalent circuit is built. The PEC-covered 3D model is then divided into five blocks. The capacitances to ground of different block combinations are extracted. Finally, the values of ohmic sheet surface resistances for each block are adjusted until the impedance characteristics of the whole 3D body model match those of the human holding a metal piece.

A. Impedance Analysis of the HMM

A setup similar to the one described in [5] is used to capture the impedances and discharge currents. This is shown in Fig. 1. For the impedance measurements, a volunteer contacts the inner pin of a subminiature version A (SMA) probe using a round metal rod while he or she stands in front of the shielded enclosure. The vector network analyzer (VNA) calibration plane is set at the end of the SMA probe. The resulting impedance, shown in Fig. 2(a), matches the result in which we published in [5].

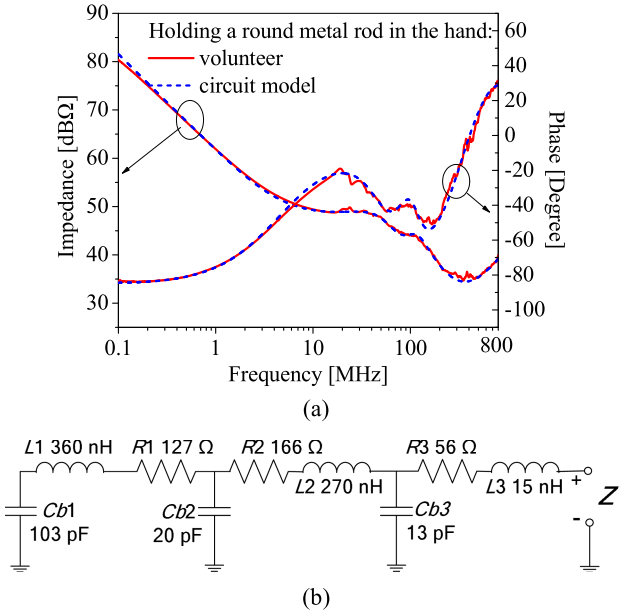

Fig. 2. Impedance measurement and equivalent circuit of a volunteer holding a round metal rod. (a) Impedance characteristics. (b) Equivalent circuit.

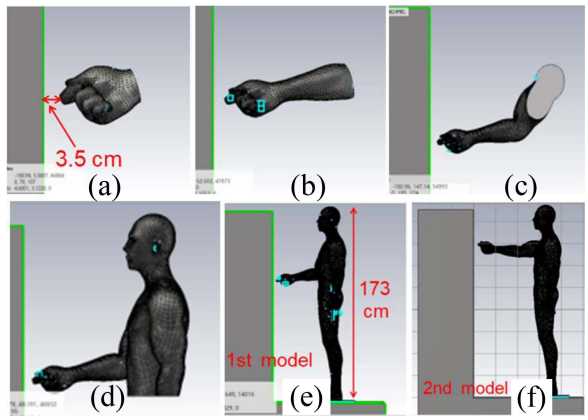

Fig. 3. 3D model and its different block combinations. (a) Hand. (b) Hand & forearm. (c) Hand & forearm & upperarm. (d) whole body with bent arm posture above waist. (e) Whole body with bent arm posture. (f) Whole body with horizontal straight arm posture.

A simple circuit model can be tuned to match the impedance of the HMM scenario, see Fig. 2(b). Components and frequency regions can be related to parts of the body and the full-size dummy. The impedance characteristics above 100 MHz are determined by Cb3, R3, and L3. The impedance characteristics below 3 MHz are decided by the sum of Cb1, Cb2, and Cb3. The impedance value around 10 MHz is approximately equal to the sum of R1, R2, and R3. Furthermore, the impedance characteristics in the 30∼100 MHz range are influenced by R2, L2, and Cb2.

B. Capacitance and Loop Inductance Extraction of a PEC-Covered 3D Model

Partial capacitances and loop inductances can be associated with parts and paths on the dummy. To achieve this, a PEC covered 3D simulation model is created. The capacitors in the circuit, shown in Fig. 2(b), can be related to the body part capacitances. These are obtained numerically. The 3D human body model is divided into the five blocks in accordance with their positions. The sum of all inductance in the circuit model is compared with the loop inductance obtained in the full wave simulation.

Step 1: A simulation model of a full size 3D human is created. As the goal is only to extract capacitances or loop inductances, using PEC as the surface is sufficient. When modeling ESD discharge currents is the goal, the impedance of the body would then need to be taken into account. The body is divided into five blocks, including the hand, the forearm, the upper arm, the waist and chest and head and the legs and feet. The blocks and combinations of them are shown in Fig. 3.

Step 2: The capacitances of the different block combinations are extracted using a CST static solver. The body model is separated from the ground by a 1.8-cm thick wooden board. The extracted capacitances and their relationship to circuit parameters are shown in Table I.

The capacitances of the circuit can be associated to the capacitances derived from a full-wave model. The full-wave model of the human body consists of blocks such as the hand, arm, body, etc. If we neglect the influence of adjacent body parts on the capacitance of one body part, we can add the capacitance values up to obtain the capacitance of a combination of parts. For example, a capacitance of around 13 pF is obtained for the combination of forearm and hand [i.e., forearm and hand in Fig. 3(b)] to the ground (without the other parts of the body). In the circuit model, this capacitance is included as Cb3. The capacitance of the combination of blocks above the waist is about 30 pF, and it is nearly equal to the sum of Cb3 and Cb2.

Step 3: The current flows from the hand via the body and back to ground. To obtain the loop inductance the model connects the feet to the reference plane. A port is set between the hand and the nearest reference ground plane. A loop inductance value of 658 nH was extracted for the models in Fig. 3(e) by the CST MWS. This value is similar to the sum of circuit inductances shown in Fig. 2(b). If the arm is stretch out, the current loop is larger. A value of 912 nH was extracted for the model in Fig. 3(f).

C. Full-Size Model Design by Using Resistive Surface Sheet

The PEC model cannot match the discharge currents. The PEC must be substituted by resistive surface sheet material. In CST MWS, an ohmic sheet surface impedance model can be used to model the dummy. It creates a surface that forms the needed impedances, and consequently leads to the correct discharge currents and transient fields. Essentially, the sheet surface impedance is similar to that of the multilayer fabric cloth used in our previous research [5], [6], where the resistance value of single-layer fabric cloth is about 400 Ω per square. In each block, the values of the ohmic sheet surface resistance need to be tuned until the impedance characteristics of the 3D model match

TABLE I
CAPACITANCE AND LOOP INDUCTANCE EXTRACTION OF A PEC COVERED 3D MODEL AND THEIR RELATIONSHIP WITH CIRCUIT PARAMETERS IN FIG. 2(b)

		Capacitance to reference plane (pF)					Loop inductance (nH)
		Hand (Fig. 3(a))	Forearm&hand (Fig. 3(b))	Whole arm&hand (Fig. 3(c))	Above waist (Fig. 3(d))	Whole body (Fig. 3(e) and (f))	
3D model	1st	7.9	12.7	17.3	30	130	658
	2nd	8	12.5	16.4	29.2	123	912
Related components in Fig. 2(b)		-	Cb3	-	Cb3+Cb2	Cb3+Cb2+Cb1	L1+L2+L3

1st model: The 3D model with bent arm posture (Fig. 3 (e));

2nd model: The 3D model with horizontal straight arm posture (Fig. 3 (f)).

TABLE II
IMPEDANCE RELATIONSHIP BETWEEN THE BODY PARTS OF THE 3D MODEL AND THE CIRCUIT COMPONENT IN FIG. 2(b)

	Frequency range			
	0.1~2 MHz	2~30 MHz	30~100 MHz	Above 100 MHz
Circuit component in Fig. 2(b)	sum of Cb1, Cb2 and Cb3	sum of R1, R2; sum of Cb1, Cb2 and Cb3	R1, L1; R2, L2 and Cb2; Cb3, R3 and L3	part regarding Cb3, R3 and L3
Body part of 3D model	whole human body		upper arm &waist & chest & head	hand & fore arm & metal rod

that of the circuit [Fig. 2(b)], i.e., the measured impedance of the real HMM scenario [Fig. 2(a)].

Based on the PEC model which was created for inductance extraction, the surface resistance of the hand and forearm are tuned at first. Here the PEC is removed in the hand and forearm and resistive sheet material is used, see Fig. 3(b). The other parts, including the wooden board, are still kept as PEC. A discrete port is defined between the front of metal rod and its nearest referencing ground plane and the impedance is calculated. The impedance above 100 MHz is dominated by Cb3, R3, and L3. The sheet resistances of the hand and forearm are tuned to match R3. The Cb3 and L3 are results of the geometry, and they are not influenced by the sheet resistance. Tuning of the sheet resistance value of the hand and the forearm leads to 5 Ω per square for the hand and 170 Ω per square for the forearm.

Second, the arm, waist, chest, and head are considered using the same methodology. Details of the geometry are shown in Fig. 3(d). They affect the impedance between 30 and 100 MHz. The impedance in this frequency range is used to tune the resistive sheet impedance in this frequency range.

Third, the sheet resistance below the waist is tuned to match the impedance below 30 MHz, see Fig. 3(e).

Table II describes the relationships of the impedances between the body parts and the circuit.

The tuned values of the sheet resistances are shown in Fig. 4(a). The simulation results of the impedances for the key design steps are given in Fig. 4(b). The corresponding geometry of each step is shown in Fig. 3(b)–(e). As shown by the red curve of Fig. 4(b), the impedance above 100 MHz is close to the reference measured result while the impedance below 10 MHz is the resistance value of forearm and hand. As the rest of the body is still PEC which is connected to ground, we see the

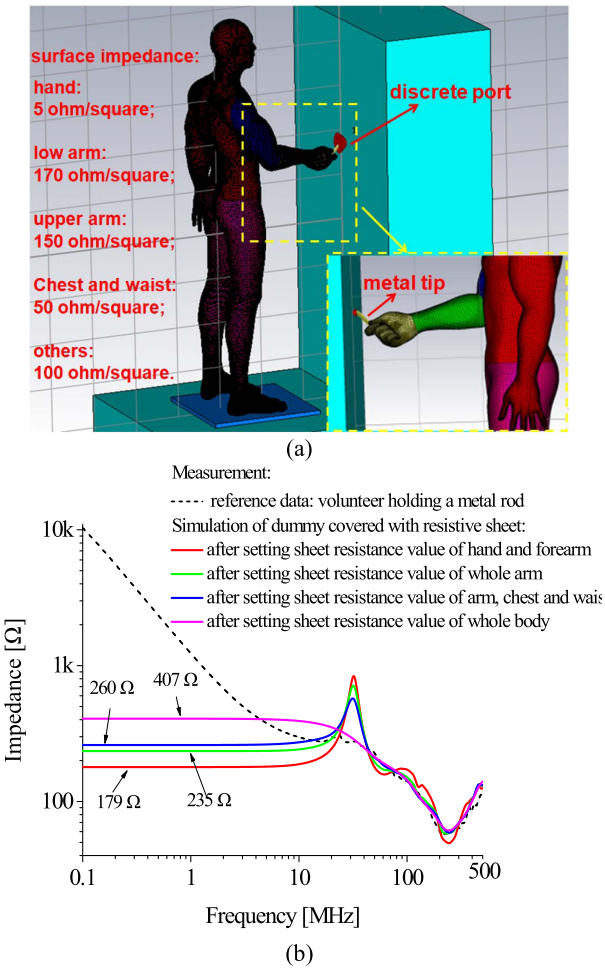

Fig. 4. 3D full-size simulation model and its adjusted impedances compared with the real HMM. (a) 3D simulation model. (b) Impedance.

resistance of the hand and forearm: 179 Ω at low frequencies. For the frequency below 10 MHz, the resistances of the whole arm and hand, the whole arm and hand and chest and waist and the whole body are 235 Ω, 260 Ω, and 407 Ω, respectively, shown by the green, blue, and pink curves of Fig. 4(b). The pink curve shows that the impedance above 30 MHz match well with the reference impedance after setting the correct sheet surface resistance values of the whole body. Finally, after setting the relative dielectric constant of wooden board under the feet back to be an insulator, the obtained final impedance shows good agreement with that of measurement from 100 kHz to

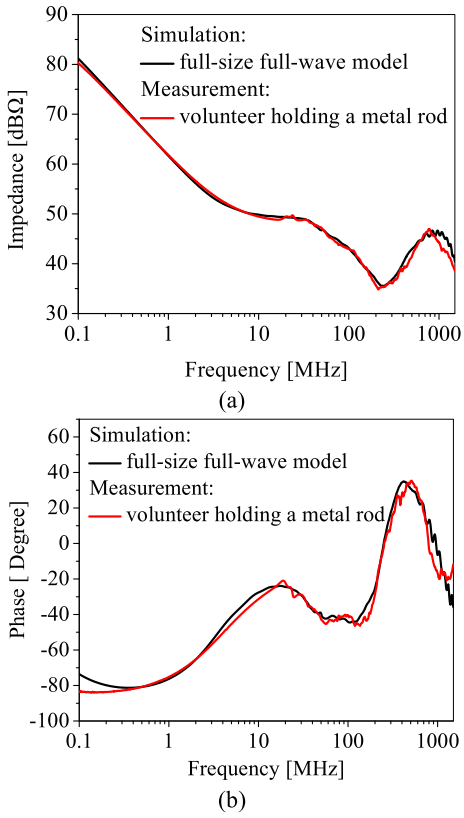

Fig. 5. Impedance comparison of the 3D full-size simulation model and the real HMM. (a) Magnitude. (b) Phase.

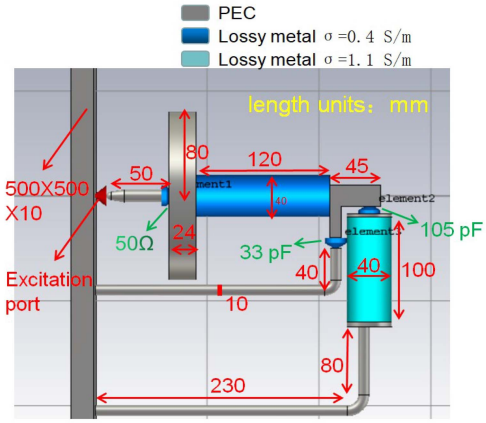

Fig. 6. Designed full-wave model of compact generator.

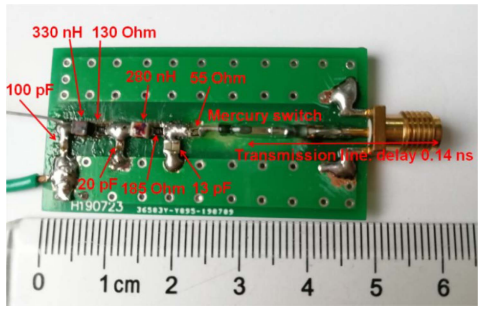

Fig. 7. Photo of the PCB-based generator [designed using the circuit of Fig. 2(b)].

1500 MHz, as shown in Fig. 5(a) and (b). Here, the transient solver of CST MWS is used to simulate the impedance and a Gaussian pulse is used as excitation.

III. Compact Generator Design

It is well-known that the IEC waveform for ESD testing does not match real human metal ESD waveforms. Most commercial ESD generators, SPICE-based and full-wave ESD generator models match the IEC ESD contact mode waveform. A compact electromagnetic model and a circuit-based simulator are proposed for achieving a better match to the actual human metal ESD waveform. These can be used to perform actual testing or numerical modeling of the response of electronic systems or suppression devices to more realistic human metal ESD waveforms.

A. Compact Full-Wave Model

The 3D compact electromagnetic model is built as depicted in Fig. 6. The design process is similar to that of the full-size model:

The main parts of the electromagnetic model are derived from the components of the circuit shown in Fig. 2(b). The capacitor Cb3 (13 pF) is represented by a metallic disk with 80 mm radius and 24 mm thickness. The resistor R3 is represented by a lumped 50 Ω resistor (shown in blue), which is located on the round metal disk. The inductor L3 is represented by around PEC rod with 50 mm length (grey). It connects the ESD generator via a port to the reference ground plane. Both R1 and R2 are represented by the cylindrical columns having 40 mm diameter, R1 is 100 mm long (green) and R2 is 120 mm (blue) long.

A lumped capacitor is used for Cb1 (105 pF). A second lumped 33 pF capacitor is placed beside the green circular column. Two metal rods connect the two capacitors to the referenced ground plane. Their lengths are tuned to approximate the effects of the inductors L1 and L2.

B. Real Circuit-Based PCB Generator

The PCB-based generator, shown in Fig. 7, uses surface mounted components arranged similar to the circuit shown in Fig. 2(b). A mercury switch initiates the discharge, allowing subnanosecond rise times. Due to the components selected, its maximal voltage of this initial design is 1 kV. The principle function is shown here. Extending to higher voltage is a straight forward procedure using high voltage capacitors and a mercury relay rated for the desired voltage.

The compact and the PCB-based simulator have been tuned to obtain similar impedances as the full-size model (Fig. 5). A comparison is shown in Fig. 8. Using a PCB trace that has a lower inductance than the apparent inductance of a metal hand held rod leads to differences in the impedance above 200 MHz. In the further works, a lumped inductor as 30 nH will be added

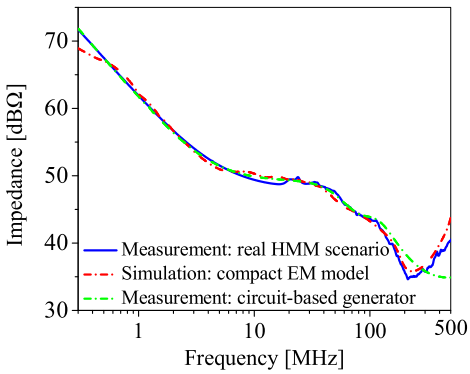

Fig. 8. Impedances of human metal ESD, compact full-wave model, and PCB-based generator.

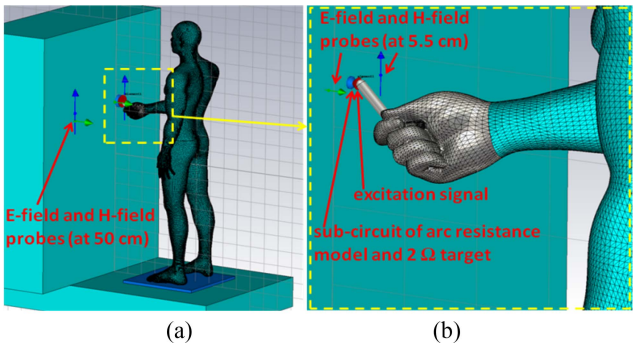

Fig. 9. Full-wave model for transient simulation in air discharge mode. (a) Complete simulation model. (b) Positions of excitation port and field probes (at 5.5 cm).

to the front of the PCB circuit. We expect that this will lead to a better impedance match above 500 MHz. The maximal voltage is limited by the mercury relay and the capacitors selected. Both can be modified for achieving up to 10 kV charge voltage.

IV. Discharge Current and Transient Field Validation

This section compares currents and transient fields of the full-wave model, the compact simulation model, and the PCB-based ESD generator for different voltages against measured HMM. The time-dependent spark resistance is included in the simulations.

A. Transient Simulation Including the Spark Resistance

CST MWS allows including a nonlinear component described by a SPICE subcircuit into the transient solver [15]. The spark model of Rompe–Weizel [23] describes the time-varying spark resistance. The simulation model is shown in Fig. 9(a). A smooth step voltage source with a 0.2 ns rise time is used to excite the transient simulation, see Fig. 9(b). The rise time of the step voltage must be less than the resulting rise time of the ESD current.

The time-dependent spark resistance, thus the rising edge of the current, depends on the voltage and the spark length. Three voltage levels, 1, 5, and 10 kV are used for validating the model.

TABLE III
Solvers of CST Used in All Simulations of This Article

Applications	Dummy model in Fig. 3(e) and (f)	Solver of CST	Reasons
Capacitance extraction	1st model and 2nd model both covered with PEC	Static solver	Solver is integrated in CST, it is convenient to use.
Loop inductance extraction	1st model and 2nd model both covered with PEC	Transient solver with Gaussian excitation	The dummy is shorted to ground by setting the wooden board as PEC. So the impedance at low frequency is determined by loop inductance.
Impedance simulation	1st Model covered with resistive surface	Transient solver with Gaussian excitation	It is appropriate for broadband simulation.
Discharge current and transient fields	1st Model covered with resistive surface	Transient solver with smooth step excitation	The time-variation arc resistance model is easy to include into MWS by using a nonlinear lumped component.

Four electric and magnetic field probes are placed at 5.5 cm and 50 cm from the discharge point, shown in Fig. 9.

In the transient simulation [15], the calculation frequency range is set as 0∼1.6 GHz to allow for the 0.2 ns rise time of the excitation signal. The hexahedral mesh is set to at least 30 cells per wavelength at 1.6 GHz. Geometrically driven, the smallest cell edge is 0.1 cm, and the largest cell edge is 0.62 cm. The model requires about 156 million cells.

Ideally, the metal rod would be placed in such a way that the distance to ground matches the spark length. In this case, however, the number of mesh cells would increase. To avoid this, a 5-mm long lumped component (blue in Fig. 9) is used to couple the 3D structure with the spark resistance model instead. It takes 16 h to simulate 50 ns using a work station (I9 9820X, 64 GB, GPU RTX 4000 8G).

B. Comparisons of Discharge Currents

The spark length is determined by the speed of approach and the statistical time lag [12]. This is also determined by surface materials and humidity. At high approach speeds and with dry air, the spark length can be reduced down to 20% of the corresponding Paschen value. We used a spark length of 0.1 mm for 1 kV, used 1.1 mm (Paschen value), 0.7 mm, and 0.2 mm for 5 kV, we used 2.7 mm (Paschen value) for 10 kV.

The simulation results are shown in Fig. 10(a)–(c). The discharge currents and their rise times at 1, 5, and 10 kV in general agree with the measurements. For the real HMM, a 2 Ω broadband current target captures the discharge current. The circuit-based PCB generator current is measured at 50 Ω. After 8 ns, the discharge currents at 1 and 5 kV agree well between measurement and simulation. Due to the influence of arc model accuracy at the high voltage level, inevitable differences exist between the simulated currents and measured currents at 10 kV.

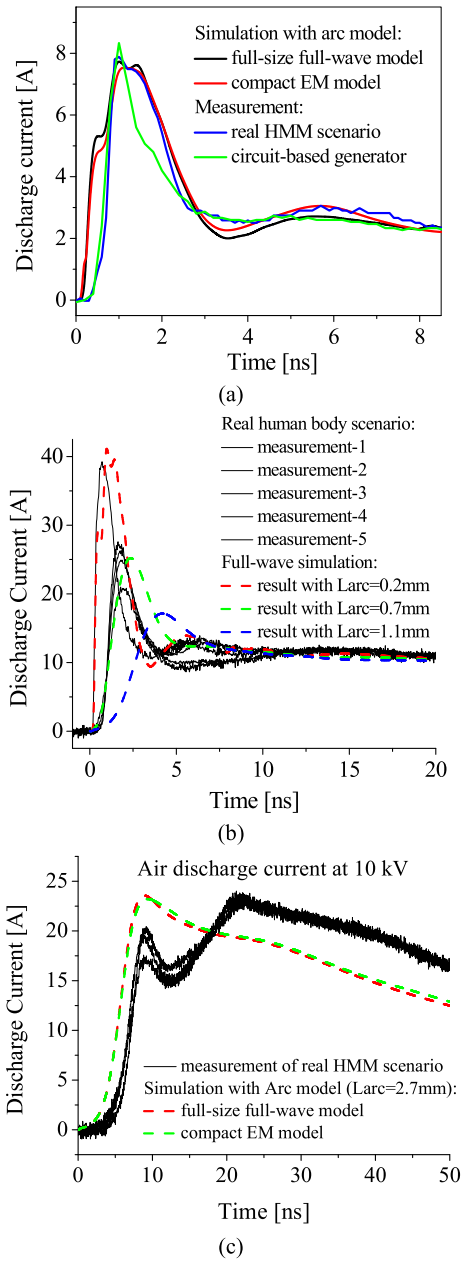

Fig. 10. Discharge current from the 3D full-wave model and the compact generator at different voltage level. (a) 1 kV. (b) 5 kV. (c) 10 kV.

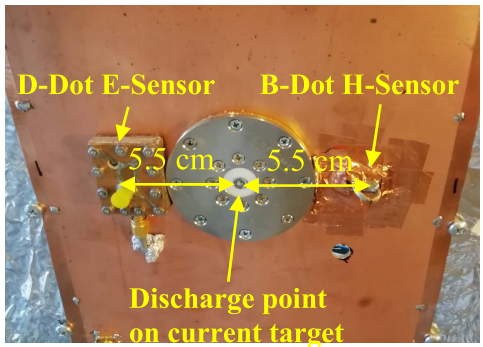

Fig. 11. Positions of D-Dot and B-Dot sensors at 5.5 cm from the discharge point.

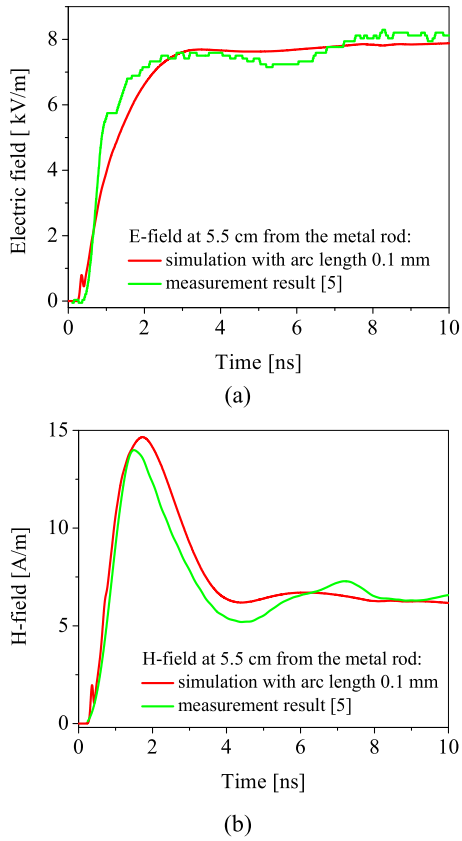

Fig. 12. E/H field comparison of air discharges of the 3D full-size model simulation and using 1 kV at 5.5 cm. (a) E-field. (b) H-field.

C. Comparisons of Transient Fields

As seen in Fig. 9, electric magnetic field probes are placed at 5.5 and 50 cm from the discharge points. These positions match the positions in the measurements, as shown in Figs. 9 and 11. The E/M fields are obtained simultaneously with the discharge currents. The measurement bandwidth of the field sensors is from 2 MHz to 2 GHz, their calibration and compensation process are described in our previous work. It is based on a 100 Ω open TEM cell [7].

A good match is achieved for 5.5 and 50 cm distance to the discharge point, see Figs. 12 and 13. This confirms the quality of the 3D full wave model.

V. Summary and Discussion of Modeling Methods and Its Applicability

In this section, the solvers of CST used in the dummy modeling are summarized, and the applicability of the proposed models is listed.

A. Solvers Summary of CST Used for Dummy Modeling

In this research work, three solvers of CST are used. The static solver is used to obtain the capacitances. In CST MWS, the transient solver is utilized to obtain the scattering parameters for

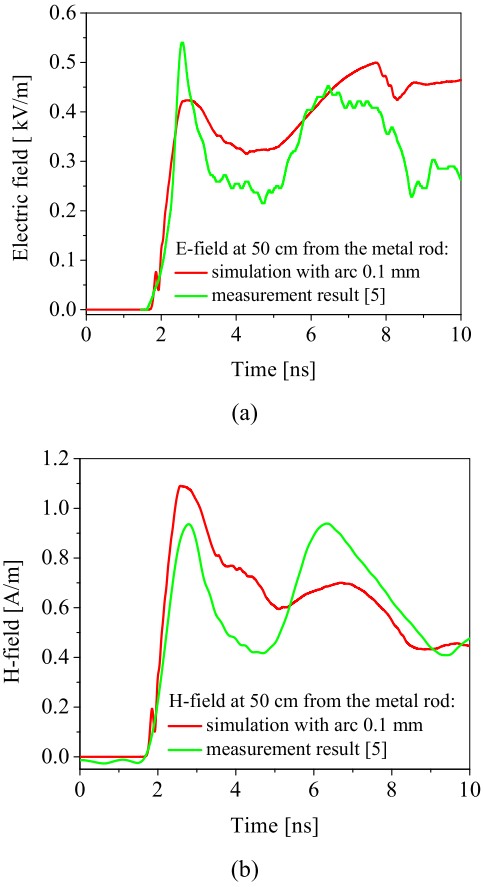

Fig. 13. E/H field comparison of air discharges of the 3D full-size model simulation and using 1 kV at 50 cm. (a) E-field. (b) H-field.

dummy, thus the impedance using a Gaussian excitation source. Transient cosimulation is also used to get time-domain response for the discharge currents and transient fields using smooth step voltage source and Rompe–Weizel's spark resistance equation. The solvers used, models, applications, and reasons are listed in Table III.

B. Applicability of the Proposed Models

The applicability of the proposed models for different applications is summarized as follows.

First, the proposed full-size full-wave dummy can be used to simultaneously predict the discharge currents and transient fields considering the time-variation arc resistance model. Furthermore, it can be used for other ESD scenarios, such as the ESD involving a set of artificial reality glasses that are connected to a body-worn processing unit. Here, it could solve for the currents on the two units and the interconnecting wires.

Second, it is known that the second hump of the current, as shown in the ESD standard, does not occur in the real human metal ESD. The proposed compact full-wave generator can be used to design a new ESD generator or to improve the design of current IEC standard generator. This design method would improve the match between the actually observed human metal ESD and the new ESD generator design.

Third, the PCB-based ESD generator can be used to characterize the transient voltage suppressor and as a source within system efficient ESD design (SEED) applications [24], [25], [26].

Fourth, the compact full wave simulator model can be used for ESD full wave simulation in which only the injected current is relevant, rather than the transient fields from the complete body. If that is needed, the full wave dummy model can be used as an excitation to the analysis of ESD risk and ESD product response.

VI. Conclusion

In this article, a full-size, full-wave human body model is designed. Based on the impedance and its equivalent circuit model of the real human body scenario, the capacitances to the ground for the different parts of 3D human body model are extracted to aid the model design process. The proposed full-wave model has the following features and advantages.

1) The values of ohmic sheet surface resistances are tuned to ensure that the impedances of model match those of the real human body.
2) The time-dependent spark resistance is directly embedded into the CST MWS. Thus, the discharge current, electric fields, and magnetic fields can be simultaneously obtained without involving a separated circuit simulator.

The proposed full-wave model is validated by comparison with the measurement results of discharge currents and transient fields. Furthermore, a compact electromagnetic full-wave model and a real circuit-based simulator based on the equivalent circuit of the real human body impedance have also been designed. Compared with the traditional standardized ESD generators, their impedance characteristics are more similar to those of the real human body. Both achieve discharge currents similar to those of the designed full-scale 3D numerical model.

The next step is to increase the voltage of the proposed circuit-based generator to 10 kV, to inject pulses from the circuit-based ESD generator into systems containing ESD protection devices following the concept of SEED.

References

[1] T. Ishida, S. Nitta, F. Xiao, Y. Kami, and O. Fujiwara, "An experimental study of electrostatic discharge immunity testing for wearable devices," in *Proc. IEEE Int. Symp. Electromagn. Compat.*, 2015, pp. 839–842.
[2] J. Zhou et al., "Characterization of ESD risk for wearable devices," *IEEE Trans. Electromagn. Compat.*, vol. 60, no. 5, pp. 1313–1321, Oct. 2018.
[3] M. Kohani, A. Bhandare, L. Guan, D. Pommerenke, and M. G. Pecht, "Evaluating characteristics of electrostatic discharge (ESD) events in wearable medical devices: Comparison with the IEC 61000-4-2 standard," *IEEE Trans. Electromagn. Compat.*, vol. 60, no. 5, pp. 1304–1312, Oct. 2018.
[4] Electromagnetic Compatibility (EMC)-Part 4-2, *Testing and Measurement Techniques-Electrostatic Discharge Immunity Test*, IEC International Standard 61000-4-2, 2008.
[5] G.-X. Luo, K. Huang, J.-C. Zhou, W. Zhang, D. Pommerenke, and J. Holliman, "Design of an artificial dummy for human metal model ESD," *IEEE Trans. Electromagn. Compat.*, vol. 63, no. 1, pp. 319–323, Feb. 2021.
[6] G.-X. Luo, K. Huang, and D. Pommerenke, "Circuit-aided dummy design for human body-worn ESD application," *IEEE Trans. Electromagn. Compat.*, vol. 64, no. 6, pp. 1820–1828, Dec. 2022.
[7] K. Wang, D. Pommerenke, R. Chundru, T. V. Doren, J. L. Drewniak, and A. Shashindranath, "Numerical modeling of electrostatic discharge generators," *IEEE Trans. Electromagn. Compat.*, vol. 45, no. 2, pp. 258–271, May 2003.

[8] S. Caniggia and F. Maradei, "Circuit and numerical modeling of electrostatic discharge generators," *IEEE Trans. Ind. Appl.*, vol. 42, no. 6, pp. 1350–1357, Nov./Dec. 2006.
[9] S. Caniggia and F. Maradei, "Numerical prediction and measurement of ESD radiated fields by free-space field sensors," *IEEE Trans. Electromagn. Compat.*, vol. 49, no. 3, pp. 494–503, Aug. 2007.
[10] D. Liu et al., "Full-wave simulation of an electrostatic discharge generator discharging in air-discharge mode into a product," *IEEE Trans. Electromagn. Compat.*, vol. 53, no. 1, pp. 28–37, Feb. 2011.
[11] D. Z. Li, S. Marathe, P. Wei, A. Hosseinbeig, and D. Pommerenke, "Full-wave simulation of system-level disruption during secondary ESD events in a smartphone," *IEEE Trans. Electromagn. Compat.*, vol. 61, no. 1, pp. 40–47, Feb. 2019.
[12] D. Pommerenke, "ESD: Transient field, arc simulation and rise time limit," *J. Electrostatics*, vol. 36, no. 1, pp. 31–54, Nov. 1995.
[13] Y. Taka, T. Ishida, and O. Fujiwara, "Waveform comparison and difference factors in discharge currents for air discharges from different ESD generators," *Elect. Eng. Jpn.*, vol. 200, no. 1, pp. 3–11, Mar. 2017.
[14] J. M. Meek and J. D. Craggs, *Electrical Breakdown of Gases*. London, U.K.: Oxford Univ. Press, 1978.
[15] CST (Computer Simulation Technology) Microwave Studio version, 2019. [Online].Available: https://www.cst.com/
[16] D. Z. Li, J. Zhou, A. Hosseinbeig, and D. Pommerenke, "Transient electromagnetic co-simulation of electrostatic air discharge," in *Proc. 39th Elect. Overstress/Electrostatic Discharge Symp.*, 2017, pp. 1–8.
[17] K. Fujita, "MNL-FDTD/SPICE method for fast analysis of short-gap ESD in complex systems," *IEEE Trans. Electromagn. Compat.*, vol. 58, no. 3, pp. 709–720, Jun. 2016.
[18] K. Fujita, J. Zhou, and D. Pommerenke, "Hybrid full-wave/circuit modelling of spark gaps and its experimental validation," *Electron. Lett.*, vol. 53, no. 7, pp. 484–486, Mar. 2017.
[19] A. Hirata et al., "Dispersive FDTD analysis of induced electric field in human models due to electrostatic discharge," *Phys. Med. Biol.*, vol. 57, no. 13, pp. 4447–4458, Jun. 2012.
[20] I. Oganezova et al., "Human body impedance modelling for ESD simulations," in *Proc. IEEE Int. Symp. Electromagn. Compat. Signal/Power Integrity*, 2017, pp. 629–633.
[21] T. Ishida, F. Xiao, Y. Kami, O. Fujiwara, and S. Nitta, "Characteristics of discharge currents measured through body-attached metal for modeling ESD from wearable electronic devices," *IEICE Trans. Commun.*, vol. 99, no. 1, pp. 186–191, Jan. 2016.
[22] J. Park, J. Lee, C. Jo, B. Seol, and J. Kim, "A proto-type ESD generator for system immunity test of wearable devices," in *Proc. 40th Elect. Overstress/Electrostatic Discharge Symp.*, 2018, pp. 1–6.
[23] D. Pommerenke and M. Aidam, "ESD: Waveform calculation, field and current of human and simulator ESD," *J. Electrostatics*, vol. 38, no. 1/2, pp. 33–51, Oct. 1996.
[24] L. Speckbacher, A. Pak, M. Gholizadeh, S. M. Mousavi, D. J. Pommerenke, and H. Gossner, "Modular measurement system for system-efficient ESD design on system and component level," *IEEE Trans. Electromagn. Compat.*, vol. 64, no. 6, pp. 1812–1819, Dec. 2022.
[25] Z. Peng et al., "Characterization and modeling of commercial ICs for system-efficient ESD design," *IEEE Trans. Electromagn. Compat.*, vol. 64, no. 6, pp. 1802–1811, Dec. 2022.
[26] J. Zhou et al., "Transient response of ESD protection devices for a high-speed I/O interface," *IEEE Trans. Electromagn. Compat.*, vol. 64, no. 4, pp. 907–914, Aug. 2022.

Guang-xiao Luo (Member, IEEE) received the B.Sc. degree in communication engineering, the M.Sc. degree in system of communication and information, and the Ph.D. degree in electrical engineering from North China Electric Power University, Beijing, China, in 2000, 2003, and 2015, respectively.

From September 2018 to July 2020, he was a Postdoctoral Researcher (supported by China Scholarship Council) with the Electromagnetic Compatibility Laboratory, Missouri University of S&T, Rolla, MO, USA. In 2003, he joined the School of Electrical and Electronic Engineering, North China Electric Power University. His research interests include circuit modeling, numerical simulations, and measurements of EMC and ESD.

Bao-Cheng Huang received the B.Sc. degree in electronic information science and technology from the North China University of Science and Technology, Tangshan, China, in 2019, and the M.Sc. degree in information and communication engineering from North China Electric Power University, Beijing, China, in 2022.

He is currently with Beijing Smart-Chip Microelectronics Technology, Company, Ltd., Beijing, China. His research interests include EMC test, modeling, and simulation at the chip, PCB, and system level.

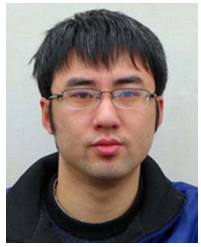

Ke Huang (Member, IEEE) received the Ph.D. degree in electrical engineering from Southwest Jiaotong University, Chengdu, China, in 2020.

From 2018 to 2019, he was the Visiting Scholar with Electromagnetic Compatibility Laboratory, Missouri University of Science and Technology, Rolla, MO, USA. He is currently a Postdoctoral Fellow with the National Maglev Transportation Engineering R&D Center, Tongji University, Shanghai, China. He has authored and coauthored more than 20 journal papers. His current research interests include arc models, arc electromagnetic interference, overvoltage, and electromagnetic compatibility of maglev transportation.

Rui Mi (Member, IEEE) received the B.S. and M.S. degrees in electrical and electronic engineering from the Missouri University of Science and Technology, Rolla, MO, USA, in 2019 and 2021, respectively. He is currently working toward the Ph.D. degree in electrical engineering with the Institute of Electronics, TU Graz, Graz, Austria.

His current research interests include RF circuits, RF nonlinear distortion effect, electromagnetic interference measurement, and design.

David Pommerenke (Fellow, IEEE) received the Diploma and the Ph.D. degrees in electrical engineering from Technical University Berlin, Berlin, Germany, in 1989 and 1995, respectively.

After working with Hewlett Packard for five years, he joined the Electromagnetic Compatibility Laboratory, Missouri University of S&T, Rolla, MO, USA, in 2001. In 2020, he moved to Graz, Austria, to join the Graz EMC Lab, Graz University of Technology, Graz, Austria, which is a joint effort with Silicon Austria Laboratory, SAL. He has authored or coauthored more than 150 journal papers and is an inventor of 13 patents. His research interests include EMC, ESD, electronics, numerical simulations, measurement methods and instrumentations.

Dr. Pommerenke is an Associated Editor for the IEEE TRANSACTIONS ON ELECTROMAGNETIC COMPATIBILITY.